RSC Advances

ROYAL SOCIETY OF CHEMISTRY

www.rsc.org/advances

RSC Advances

COMMUNICATION

Fluorescent Genipin Cross-linked REDV-Conjugated Polymeric Microbubbles for Human Vascular Endothelial Cells (HVECs) Targeting†

Zhe Liu*[a], Changcan Shi[a], Yihong Li[a], Yuanhui Song[a], Qien Xu[a]

Polymeric microbubbles modified with chitosan and genipin were fabricated *via* emulsification, electrostatic interaction and cross-linking to afford intrinsic fluorescence. REDV peptides were conjugated to achieve HVECs active targeting. The degradation, cytotoxicity and targeting features endowed them potential candidates in early molecular diagnosis for cardiovascular diseases.

In past decades, the morbidity of vascular diseases have rapidly increased and become one of the major causes of death throughout the world.[1,2] The early detection and diagnosis at molecular and cellular level is therefore of great importance to the final successful treatment.[3,4] Several biomarkers, e.g. endoglin, $\alpha_v\beta$ integrins and vascular endothelial growth factor receptors (VEGFRs) have been found over-expressed at the early stage of cardio- and cerebrovascular diseases.[5-7] Conjugating these biomarkers to micro/nano particles (molecular probes or therapeutic vehicles) is a key strategy for not only highly specific diagnosis but also targeting therapy. Nevertheless, some challenges such as intimal hyperplasia, thrombosis and low-term patency rate have been encountered especially during the course of therapy, which force scientists into taking effective measures to improve biocompatibility of probes/vehicles by structural or chemical modifications.[8-10] Collagen, heparin, gelatine, silk fibre, poly(ethylene glycol) and zwitterionic poly norbornene have been widely used to enhance the hydrophilicity and hemo-compatibility.[11-17] Besides that, bioactive peptides such as Arg-Glu-Asp-Val (REDV) can be incorporated with polymeric carriers for selective recognition and specific binding to endothelial cells (ECs) to prevent the formation of thrombosis.[18-22] By means of boosting ECs selectivity and affinity, diagnostic or therapeutic agents can be precisely anchored on the lesion to achieve following treatment convenience.

Recently, polymeric gas-filled microbubbles as contrast agents have attracted emerging attention in ultrasound imaging which is a powerful tool for non-invasive and real-time diagnosis and image-guided therapy of vascular diseases.[23-25] Meanwhile, ultrasound is also of great value for visualizing plaque neovascularization which causes plaque progression, instability and other fatal atherosclerotic events.[26] By utilizing inertial or non-inertial ultrasound cavitation, vascular lesions (e.g. thrombosis and atherosclerosis) can be physically cured.[27,28] A chemotherapy strategy is to use hybrid microbubble-based agents encapsulated with therapeutic payloads in ultrasound-triggered microbubble destruction (UTMD) to achieve long-term and controllable treatment.[29,30] Thus, the fabrication of functional polymeric microbubbles to serve multiple biomedical purposes, including bio-imaging, diagnosis and targeting therapy will provide unprecedented opportunities for successful treatment of vascular diseases.

Various polymeric microbubbles have been designed and prepared by FDA-approved biocompatible and non-toxic materials such as poly lactic acid (PLA), poly lactic-co-glycolic acid (PLGA), poly acrylate (PA), etc.[31-34] To serve multimodal imaging (e.g. ultrasound and fluorescence imaging) and enhance the diagnostic sensitivity, fluorescent building blocks are always incorporated in the polymeric microbubbles.[35,36] However, considering that most fluorescent dyes are cytotoxic and difficult to clearance out of normal organs *in vivo*, biocompatible cross-linked polymers with intrinsic fluorescence are alternative candidates. In this context, genipin derived from the *Gardenia Jasminoides Ellis* was applied as a natural biocompatible cross-linker to yield fluorescent poly butyl cyanoacrylate (PBCA) microbubbles prepared *via* emulsion polymerization followed by chitosan (CS) surface-coating. In order to endow HVECs active targeting capability, REDV as HVECs-specific peptides were covalently conjugated for selective binding to achieve PBCA-CS-REDV-MBs (Scheme 1).

To the best of our knowledge, these REDV-conjugated polymeric microbubbles for active targeting human vascular endothelial cells have not been reported before although the targeting mechanism of REDV selective recognition by $\alpha_4\beta_1$ integrin receptors expressed on the endothelial cell membranes has been well elucidated.[18] Their degradation,
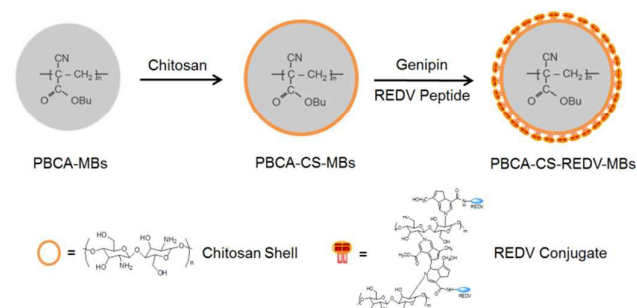
Scheme 1. Illustrative fabrication of HVECs-targeting polymeric microbubbles *via* chitosan surface-coating, genipin cross-linking and REDV peptide conjugation.

cytotoxicity and HVECs active targeting performance were evaluated which indicated that the as-fabricated PBCA-CS-REDV-MBs are a potential candidate in bio-imaging and early molecular diagnosis for vascular diseases. Furthermore, these hybrid fluorescent polymeric microbubbles are capable of embedding thrombolytic drugs to act as multifunctional theranostic agents for *in vivo* ultrasound image-guided treatment.

First of all, microbubbles for ECs active targeting were prepared *via* emulsion polymerization of butyl cyanoacrylate (BCA) followed by chitosan surface-coating and REDV conjugation. *In-situ* polymerization of BCA afforded pure polymeric microbubbles with negative zeta potential (-30±5.9 mV). By electrostatic interaction, chitosan coating could be readily accomplished on PBCA-MBs surface to give positively charged PBCA-CS-MBs (55±5.9 mV). While the surface charge has converted completely, the average sizes of PBCA-MBs and PBCA-CS-MBs didn't change significantly (3.4±1.3 μm vs. 3.7±1.0 μm) as shown in Figure 1A and B. As a natural biocompatible cross-linking agent, genipin displays 5000-10000 times less toxicity than traditional cross-linker

glutaraldehyde, and won't lead to harsh inflammatory response.[37,38] More importantly, genipin-mediated cross-linking can introduce intrinsic fluorescence due to the resulted conjugation system, which will enable fluorescent cell labelling and imaging. Based on these advantages, genipin was used to react with the amino groups of chitosan on the surface of PBCA-CS-MBs following which REDV were covalently conjugated to afford PBCA-CS-REDV-MBs. It is interestingly found that after cross-linking, the viscosity of microbubbles has been increased and they were stabilized by the tight cross-linked structure. Figure 1C and D showed the SEM images before and after genipin cross-linking, and it was observed that most of the microbubbles after cross-linking were maintained intact and displayed the real morphology instead of thoroughly bursting. This can be explained that the cross-linked structure between chitosan and genipin composed a contracted network like a bird nest on the microbubble surface that greatly boosted their tightness in spite of a slight shrinkage. The surface rough morphology resulted from polymeric materials were characterized with high magnitude SEM visualization which could complementarily verify the microbubble sizes (Figure 1E and F).

The FT-IR spectra were obtained to identify the successful surface-coating and conjugation between chitosan, genipin and REDV peptides. Pure PBCA-MBs with a bare surface gave no characteristic peaks, but a broad absorption band from 3300 cm^{-1} to 3340 cm^{-1} were identified for PBCA-CS-MBs as the assignment of primary amine (-NH$_2$) and secondary amide (-NH-) groups in chitosan (Figure 2A and B). Because of strong electrostatic adherence, positively charged chitosan was coated on the PBCA-MBs surface, and therefore the absorption of amino peaks was apparently increased. However, most amino groups were consumed after genipin cross-linking and REDV conjugation, and thus a significant fade-off of amino absorption peaks indicated that PBCA-CS-REDV-MBs were finally formed (Figure 2C). Obvious absorption peaks of cyano groups (-CN) were also observed at 2250 cm^{-1} in all different microbubbles which validated the composition of PBCA components (Figure 2A-C). The introduction of genipin to cross-
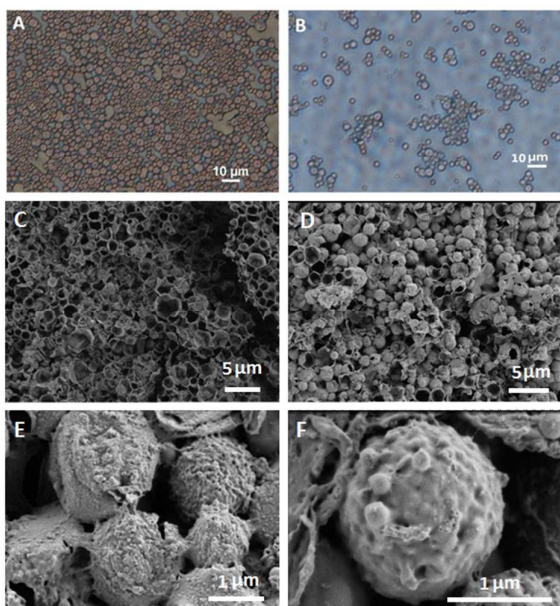

Figure 1. Microscopy of gas-filled MBs before (A) and after (B) chitosan surface-coating. SEM images of MBs before (C) and after (D) genipin cross-linking. High magnitude visualization of several (E) and single (F) PBCA-CS-REDV-MBs.
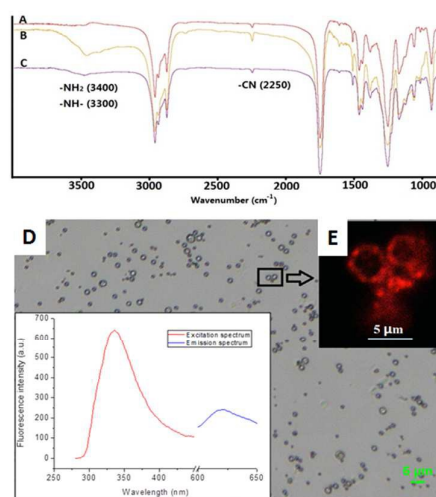

Figure 2. Characterization of PBCA-based microbubbles: FT-IR spectra of PBCA-MBs (A), PBCA-CS-MBs (B) and PBCA-CS-REDV-MBs (C); bright-field (D) and

confocal laser scanning microscopy (E) of genipin cross-linked PBCA-CS-REDV-MBs. (Inset: excitation and emission spectrum)

link chitosan not only enhances the microbubble framework but also endows them with the intrinsic fluorescence, which provides convenience for bio-imaging and real-time detection with high sensitivity. In order to characterize the optical features, the excitation and emission spectra were acquired (Figure 2D inset). PBCA-CS-REDV-MBs exhibited a maximum excitation at the wavelength of 349 nm, and a characteristic emission peak at the wavelength of 625 nm in the spectra. Compared with the optical properties of genipin alone, this excitation and emission evidence also synergistically supported that genipin and chitosan had cross-linked together to yield the red fluorescence. With the confocal laser scanning microscopy (CLSM), the fluorescent PBCA-CS-REDV-MBs could be clearly visualized as compared to a bright field image (Figure 2D and E).

Next, a gel retardation assay between PBCA-CS-REDV-MBs and pEGFP was employed to evaluate the binding capability of REDV-conjugated microbubbles as potential DNA carriers for gene transfection and therapy. Since the size of pEGFP-binded microbubbles is too large to diffuse through the agarose matrix, only the plasmids which do not bind onto the surface of microbubbles are able to migrate to the positive electrode in the same manner as the naked plasmid does.[39] Before the gel retardation assay, PBCA-CS-REDV-MBs/pEGFP complexes with different v/v ratios were incubated at room temperature. The image of gel retardation assay was obtained as shown in Figure 3A. The results clearly indicated that plasmids could not totally bind REDV-conjugated microbubbles until the v/v ratio was increased to 1:1. By electrostatic interactions of positive microbubbles and negative pEGFP, the PBCA-CS-REDV-MBs could condensate plasmids efficiently. These findings implied that the PBCA-CS-REDV-MBs might be suitable carriers to effectively load therapeutic genes for transfections and therapy.

To evaluate the degradation behaviour, PBCA-CS-REDV-MBs was tested in PBS (pH=7.4) at 37 °C under constant shaking at 30 rpm. After 45 days, the relative residual weight of PBCA-CS-REDV-MBs decreased to 93.4%, while that of non-targeting PBCA-MBs decreased to 98.2%. Thus PBCA-CS-REDV-MBs showed a relatively faster weight loss rate than PBCA-MBs. According to Figure 3B, the degradation process of PBCA-CS-

deviations (n=3); (C) Relative cell viability for PBCA-CS-REDV-MBs incubated with EA.hy926 cells for 48h at different microbubble concentrations.

REDV-MBs exhibited two stages. During the initial 15 days, the residual weight decreased sharply, which might be attributed to the rapid dissolution of chitosan that had not cross-linked with genipin on the microbubble surface. The second stage is that the PBCA shell of microbubbles displayed very slow degradation rate of residual weight. Moreover, during the whole degradation assay, only 1.8% of PBCA-MBs weight decreased which indicated that these microbubbles are stable enough in PBS to act as mid-term disintegration-resistant drug or gene carriers.

Since the cytotoxicity associated with microbubbles served as ultrasound contrast agents has aroused considerable attention, the toxicity of PBCA-CS-REDV-MBs was evaluated by MTT assay. As shown in Figure 3C, PBCA-CS-REDV-MBs only showed mild cytotoxicity (cell viability >80%) even at high concentration (8 μL MBs/100 μL medium). Low cytotoxicity is also one of the prerequisites for their *in vivo* application. Considering that the pure PBCA microbubbles have been reported as effective ultrasound contrast agents,[34] our present findings strongly manifested that the REDV-conjugated targeting microbubbles can be used as a sensitive and biocompatible imaging tool as well as a stable therapeutic platform with acceptable cytotoxicity at low doses.

So as to investigate the HVECs active targeting capability, PBCA-CS-REDV-MBs were incubated with ECs and smooth muscle cells (SMCs) in the culture medium, respectively. REDV peptide was specifically recognized by integrin $\alpha_4\beta_1$ receptors expressed on the cyto-membrane surface of ECs but not on SMCs. Therefore, the targeting PBCA-CS-REDV-MBs may be expected to attach onto the ECs efficaciously. This speculation was verified in the assay (Figure 4). After 12 h of incubation, a number of PBCA-CS-REDV-MBs had been attached on the ECs.

Figure 4. Active targeting assay of REDV-peptide conjugated microbubbles. At different time points, targeting capability of PBCA-CS-REDV-MBs binding to ECs 1) and SMCs 2) displayed a significant difference, respectively; 3) Red fluorescence
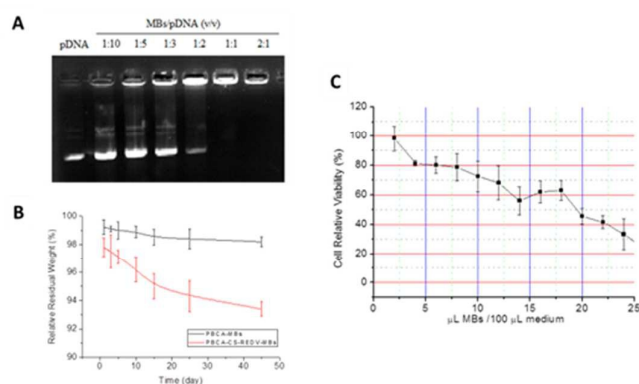

Figure 3. (A) Agarose gel electrophoresis of MBs/pEGFP complexes at different v/v ratios; (B) Residual weight loss of non-targeting PBCA-MBs and targeting PBCA-CS-REDV-MBs in PBS (pH=7.4) at 37°C. Error bars represent the standard
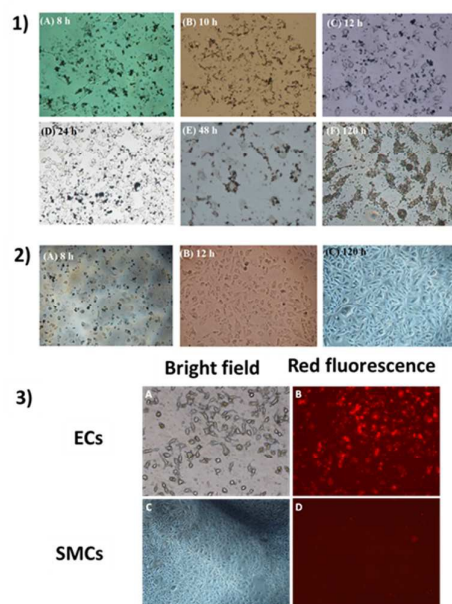
images of PBCA-CS-REDV-MBs/ECs vs. PBCA-CS-REDV-MBs/SMCs after 120 h of incubation.

The specific binding capability proved to be strong enough so that even after 120 h of incubation a large majority of targeting microbubbles were still attached (Figure 4-1). In comparison to the negative control, PBCA-CS-REDV-MBs cultured with SMCs under the same condition showed that almost none of targeting microbubbles were binding on the SMCs (Figure 4-2). With the fluorescence microscope, the specific binding of PBCA-CS-REDV-MBs could be clearly observed in both the bright field and red fluorescence window (Figure 4-3). Most of the targeting microbubbles were identified integrity. In contrast, nearly obscure red fluorescence could be visualized for the targeting PBCA-CS-REDV-MBs on the SMCs which was in good accordance with the HVECs targeting nature.

In conclusion, novel polymeric fluorescent microbubbles consist of poly butyl cyanoacrylate, chitosan and genipin were prepared *via* emulsion polymerization followed by electrostatic interaction of chitosan and genipin cross-linking. In order to endow HVECs active targeting, REDV were conjugated to achieve PBCA-CS-REDV-MBs. The structure and fluorescent properties were well characterized, and the degradation, cytotoxicity and outstanding HVECs targeting performance were evaluated which confirmed that the as-fabricated PBCA-CS-REDV-MBs are a potential candidate in bio-imaging and early molecular diagnosis of vascular diseases. Further drug or gene encapsulation and ultrasound-triggered release on diseased lesions using these targeting PBCA-CS-REDV-MBs as both contrast agents and therapeutic vehicles are underway in our laboratory, which will promisingly make them a powerful theranostic platform.

Notes and references

1   M. A. Creager, *Nat. Rev. Cardiol.*, 2014, **11**, 635.
2   A. M. Manley and S. E. Reck, *Med. Clin. North Am.*, 2013, **97**, 1077.
3   D. Dallmeier and W. Koenig, *Best Pract. Res. Clin. Endocrinol. Metab.*, 2014, **28**, 281.
4   S. S. Xu, S. Alam and A. Margariti, *Curr. Vasc. Pharmacol.*, 2014, **12**, 77..
5   C. Stratz, M. Amann, D. D. Morrow, F. J. Neumann and W. Hochholzer, *Cardiol. Rev.*, 2012, **20**, 111.
6   P. T. Dijke, M. J. Goumans and E. Pardali, *Angiogenesis*, 2008, **11**, 79.
7   B. Shen, X. Zhao, K. A. O'Brien, A. Stojanovic-Terpo, M. K. Delaney, K. Kim, J. Cho, S. C. Lam and X. Du, *Nature*, 2013, **503**, 131.
8   K. Zhang, T. Liu, J. A. Li, J. Y. Chen, J. Wang and N. Huang, *J. Biomed. Mater. Res. A*, 2014, **102**, 588.
9   R. S. Smith, Z. Zhang, M. Bouchard, J. Li, H. S. Lapp, G. R. Brotske, D. L. Lucchino, D. Weaver, L. A. Roth, A. Coury, J. Biggerstaff, S. Sukavaneshvar, R. Langer and C. Loose, *Sci. Transl. Med.*, 2012, **4**, 153ra132.
10 S. H. Ye, Y. S. Jang, Y. H. Yun, V. Shankarraman, J. R. Woolley, Y. Hong, L. J. Gamble, K. Ishihara and W. R. Wagner, *Langmuir*, 2013, **29**, 8320.
11 J. Burck, S. Heissler, U. Geckle, M. F. Ardakani, R. Schneider, A. S. Ulrich and M. Kazanci, *Langmuir*, 2013, **29**, 1562.
12 W. Gong, D. Lei, S. Li, P. Huang, Q. Qi, Y. Sun, Y. Zhang, Z. Wang, Z. You, X. Ye and Q. Zhao, *Biomaterials*, 2016, **76**, 359.
13 T. E. Deglau, T. M. Maul, F. S. Villanueva and W. R. Wagner, *J. Vasc. Surg.*, 2012, **55**, 1087.
14 C. E. Hagemeyer, K. Alt, A. P. Johnston, G. K. Such, H. T. Ta, M. K. Leung, S. Prabhu, X. Wang, F. Caruso and K. Peter, *Nat. Protoc.*, 2015, **10**, 90.
15 G. Tae, M. Scatena, P. S. Stayton and A. S. Hoffman, *J. Biomater. Sci. Polym. Ed.*, 2006, **17**, 187.
16 H. Xu, J. L. Kaar, A. J. Russell and W. R. Wagner, *Biomaterials*, 2006, **27**, 3125.
17 E. Elacqua, D. S. Lye and M. Weck, *Acc. Chem. Res.*, 2014, **47**, 2405.
18 X. Ren, Y. Feng, J. Guo, H. Wang, Q. Li, J. Yang, X. Hao, J. Lv, N. Ma and W. Li, *Chem. Soc. Rev.*, 2015, **44**, 5680.
19 Y. Wei, J. X. Zhang, Y. Ji and J. Ji, *Colloids Surf. B Biointerfaces*, 2015, **136**, 1166.
20 Y. Wei, Y. Ji, L. L. Xiao, Q. K. Lin, J. P. Xu, K. F. Ren and J. Ji, *Biomaterials*, 2013, **34**, 2588.
21 Y. Wei, J. Zhang, H. Li, L. Zhang and H. Bi, *J. Biomater. Sci. Polym. Ed.* 2015, **26**, 1357.
22 X. Cai, *Expert Rev. Cardiovasc. Ther.*, 2006, **4**, 789.
23 X. Xiong, F. Zhao, M. Shi, H. Yang and Y. Liu, *J. Biomater. Sci. Polym. Ed.*, 2011, **22**, 417.
24 P. Palekar-Shanbhag, M. M. Chogale, S. V. Jog and S. S. Gaikwad, *Curr. Drug. Deliv.*, 2013, **10**, 363.
25 M. Azmin, C. Harfield, Z. Ahmad, M. Edirisinghe and E. Stride, *Curr. Pharm. Des.*, 2012, **18**, 2118.
26 D. Staub, A. F. Schinkel, B. Coli, A. F. van der Steen, J. D. Reed, C. Krueger, K. E. Thomenius, D. Adam, E. J. Sijbrands, F. J. ten Cate and S. B. Feinstein, *JACC Cardiovasc. Imaging*, 2010, **3**, 761.
27 Y. H. Chuang, P. W. Cheng, S. C. Chen, J. L. Ruan and P. C. Li, *Ultrason. Imaging*, 2010, **32**, 81.
28 K. E. Hitchcock and C. K. Holland, *Stroke*, 2010, **41**, S50.
29 Z. Y. Chen, F. Yang, Y. Lin, J. S. Zhang, R. X. Qiu, L. Jiang, X. X. Zhou and J. X. Yu, *Curr. Gene Ther.*, 2013, **13**, 250.
30 Y. Zhang, S. Chang, J. Sun, S. Zhu, C. Pu, Y. Li, Y. Zhu, Z. Wang and R. X. Xu, *Mol. Pharm.*, 2015, **12**, 3137.
31 F. Cavalieri, M. Zhou, M. Tortora, B. Lucilla and M. Ashokkumar, *Curr. Pharm. Des.*, 2012, **18**, 2135.
32 N. Teraphongphom, P. Chhour, J. R. Eisenbrey, P. C. Naha, W. R. Witschey, B. Opasanont, L. Jablonowski, D. P. Cormode and M. A. Wheatley, *Langmuir*, 2015, **31**, 11858.
33 C. Niu, Z. Wang, G., Lu, T. M. Krupka, Y. Sun, Y. You, W. Song, H. Ran, P. Li and Y. Zheng, *Biomaterials*, 2013, **34**, 2307.
34 Z. Liu, T. Lammers, J. Ehling, S. Fokong, J. Bornemann, F. Kiessling and J. Gaetjens, *Biomaterials*, 2011, **32**, 6155.
35 A. Barrefelt, Y. Zhao, M. K. Larsson, G. Egri, R. V. Kuiper, J. Hamm, M. Saghaflan, K. Caidahl, T. B. Brismar, P. Aspelin, R. Heuchel, M. Muhammed, L. Dahne and M. Hassan, *Biochem. Biophys. Res. Commun.*, 2015, **464**, 737.
36 C. E. Schutt, S. Ibsen, M. Benchimol, M. Hsu and S. Esener, *Opt. Lett.*, 2015, **40**, 2834.
37 V. M. Bispo, A. A. Mansur, E. F. Barbosa-Stancioli and H. S. Mansur, *J. Biomed. Nanotechnol.*, 2010, **6**, 166.
38 C. Wang, T. T. Lau, W. L. Loh, K. Su and D. A. Wang, *J. Biomed. Mater. Res. B Appl. Biomater.*, 2011, **97**, 58.
39 M. Elfinger, C. Pfeifer, S. Uezquen, M. M. Golas, B. Sander, C. Maucksch, H. Stark, M. K. Aneja and C. Rudolph, *Biomacromolecules*, 2009, **10**, 2912.

Graphical Abstract